Measuring spatially extended density profiles using atom-cavity collective strong coupling to higher-order modes

M. Niranjan,[1,*] Sourav Dutta,[1,2] Tridib Ray,[1,3] and S. A. Rangwala[1]

[1]*Raman Research Institute, C.V. Raman Avenue, Sadashivanagar, Bangalore 560080, India*
[2]*Tata Institute of Fundamental Research, 1 Homi Bhaba Road, Navy Nagar, Colaba, Mumbai 400005*
[3]*Light-Matter Interactions Unit, Okinawa Institute of Science and Technology Graduate University, Onna, Okinawa 904-0495, Japan*

The collective strong coupling of rubidium atoms in a magneto-optical trap (MOT) to the Laguerre-Gaussian (LG) modes of a Fabry-Pérot cavity is investigated. Bright and dark ^{85}Rb MOT atoms are prepared at the geometric center of the cavity, and the vacuum Rabi splitting (VRS) of the collectively coupled atom-cavity system is measured for LG_{l0} ($l = 0, 1, 2, 3$) modes. The atom number coupled to the cavity mode depends on the overlap of the atomic density distribution and the specific spatial mode function, which is reflected in the measured VRS spectrum. The known mode function and the measured VRS can then be used to test whether the atomic density distribution in the experiment is Gaussian or uniform. A simple theoretical model for this process is described, and the experimental measurements are found to be in close agreement with the model.

I. INTRODUCTION

Optical Fabry-Pérot (FP) cavities, when coupled to a cold, dilute gas of atoms, can be used to probe, detect, manipulate, or even trap atoms or molecules [1–19]. For ultracold trapped atoms, the line broadening due to atomic motion and trapping fields are small enough to allow the ensemble of cold atoms that are contained within the cavity mode volume to couple effectively with the optical cavity of moderate finesse. In many hybrid traps with cavities [3,10–12,18,20–30], where entire ensembles of the trapped species are required to be overlapped with the cavity mode, the cavity mode volume is large. This large mode volume makes single-atom strong coupling very challenging, while collective strong coupling is achievable. In this article, we use atom-cavity collective strong coupling with higher-order cavity modes to measure the density and number of atoms for the ensemble probed by the cavity mode.

The interaction of the cavity and atomic state results in the lifting of the degeneracy between (a) the excited atom and the empty cavity mode and (b) the ground-state atom and the occupied cavity mode [31,32]. The experimental manifestation of this phenomenon is seen as a frequency splitting about the atomic resonance, in the transmission of a weak probe beam. When the condition $g > \kappa, \gamma$ is satisfied, this splitting can be resolved in a measurement and is known as vacuum Rabi splitting (VRS) [23,33,34]. Here, g is the rate at which the cavity mode and the atom exchange excitation, κ is the rate at which cavity mode loses photons, and γ is the photon loss rate due to spontaneous emission from the atom coupled to the cavity. This has been observed both with single atoms [35–40] and with a collection of trapped atoms (or

ions) [18,21,22,24,26,29,30,41,42] within a high-finesse cavity. Collective strong coupling with higher-order transverse-electromagnetic (TEM) cavity modes in a multimode cavity has been demonstrated [29]. In this study we use individual higher-order Laguerre-Gaussian (LG) modes with cylindrical symmetry within the cavity to make measurements on atom numbers and their density profiles.

We prepare a magneto-optical trap (MOT) of ^{85}Rb atoms, which is well overlapped with the mode of a medium finesse, near confocal FP cavity. The coupling of both a bright MOT and a dark MOT to the fundamental and higher-order LG mode is studied experimentally. The fluorescence of the bright MOT is recorded on a calibrated photomultiplier tube (PMT1) and on a CCD camera to determine the atom number and density distribution, respectively. The VRS calculated using the experimental density as input and the measured VRS for the different LG_{l0} modes are in very good agreement. This validates the VRS measurement for the determination of the atomic density. On the other hand, the atoms in a dark MOT are trapped and shelved in the lowest hyperfine $F = 2$ level and do not interact with the cooling or repumping laser beams. In this case, the *in situ* atomic density cannot be determined via the above fluorescence measurements, but the cavity measurement can be used to estimate the density. However, this requires the VRS measurement to be performed for different LG_{l0} modes. The atom-cavity coupling is investigated for the cylindrically symmetric Laguerre-Gauss LG_{00}, LG_{10}, LG_{20}, and LG_{30} modes. As each of these modes has a different spatial distribution, the density variation of the trapped atoms integrated along the cavity axis can now be explicitly measured, assuming cylindrical symmetry.

The dependence of VRS on the choice of the transverse mode of the cavity allows and extends the utilization of FP cavities for measurements. In particular, the ability to estimate the *in situ* density profile of atoms (or molecules or ions in future experiments) in optically dark and steady-state traps
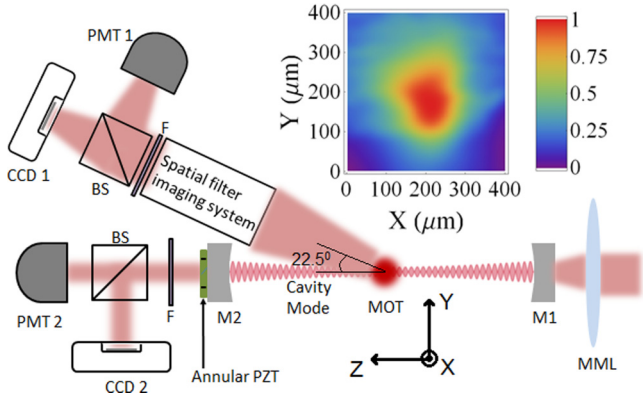
*niranjan@rri.res.in

FIG. 1. Schematic of experiment. MML is a mode-matching lens used for coupling light to the FP cavity, F is an optical bandpass filter to block any stray light of frequencies far from ω_a, BS is a beam splitter, PMT1 and PMT2 are photomultiplier tubes, and CCD1 and CCD2 are imaging cameras. The cavity resonant frequency ω_c of a particular transverse mode is matched with ω_a by adjusting the cavity length using the annular PZT, and the cavity probe laser frequency ω_p is scanned around ω_a. Inset: The contour plot for the density distribution of the ^{85}Rb MOT atoms which fluoresce with natural transition frequency ω_a are imaged by CCD1.

while using minimal probe intensities can be used advantageously in hybrid trap experiments [11,39,43,44]. In what follows, we first describe the experimental system and use the system-specific numbers and atomic parameters to model the atom-cavity collective strong coupling as a function of different transverse modes, present the results of measurements, and compare the experimental results with the theoretical model, which shows very good agreement.

II. EXPERIMENTAL DETAILS AND PARAMETERS

The experiment has a near-confocal FP cavity with mirrors with a radius of curvature of 50 mm placed at a distance of $L = 45.7$ mm, which allows us to create a MOT within the cavity as shown in Fig. 1. The mode waist $\omega(0)$ for the LG_{00} mode for the above parameters is 78 μm. The cavity has a finesse of $\mathcal{F} \approx 600$, and its length can be tuned across a few free spectral ranges with a ring-shaped piezoelectric transducer (PZT) on which one of the cavity mirrors is mounted. Details of the full hybrid trap arrangement can be found in previous experimental work [18,29,43,45–48]. The PZT allows tuning the resonant frequency of a particular LG mode of the cavity ω_c to the atomic transition frequency ω_a. The frequency of the cavity in-coupled probe light ω_p is scanned across ω_a, and the transmission signal of the probe light through the cavity is measured by a photomultiplier tube, PMT2. Although the cavity is not locked, the frequency scan of the probe frequency is much faster than the drift rate of the cavity once the cavity resonance condition is manually set. The drift during one full set of measurements is calculated to be less than ± 1 MHz, which can affect the measured VRS by up to $+0.5$ MHz. This is calculated using the formalism of Gripp *et al.* [49]. This effect is less than the natural linewidth of atoms and is smaller than the statistical error bars on measurements. The frequencies relevant to the experiment are
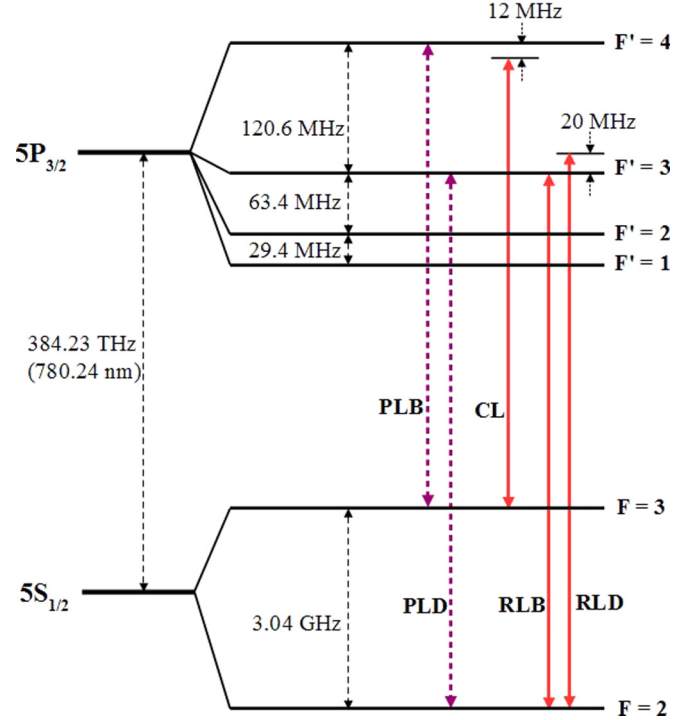

FIG. 2. The relevant ^{85}Rb energy levels and the transitions used in the experiment are illustrated. Here, CL is the cooling laser, RLB and RLD are the repumping lasers for the bright MOT and the dark MOT, respectively. The probe lasers for the bright-MOT and the dark-MOT VRS, PLB, and PLD, are scanned across the identified transitions.

illustrated in Fig. 2. The PMT measures a signal in the form of a single transmission peak at ω_c when the cavity is empty, while, with the MOT atoms in the cavity, the transmission is modified to shows two peaks, as shown in Fig. 3, separated by the VRS frequency interval given by $2\hbar g_{lm} \propto \sqrt{N_{lm}}$, where g_{lm} is the collective coupling of atoms and N_{lm} is the number of atoms coupled to the cavity mode LG_{lm}. Below we measure the VRS for the atomic distribution using the various LG_{l0} modes [18,26,29,32,41,50,51].

For a bright MOT (which has atoms in both the ground and electronically excited states at any instant), the repumping beams are combined with all six cooling beams, and for the dark MOT (where the central MOT atoms are not repumped and so are optically pumped into the dark ground state), two hollow repumping beams with a dark spot with a diameter of 2 mm in the center are combined with two of the horizontal cooling beams [43]. To measure VRS due to bright-MOT atoms, the cavity probe frequency ω_p is scanned across the $F = 3$ to $F' = 4$ atomic transition. On the other hand, for measuring VRS due to dark-MOT atoms, ω_p is scanned across the $F = 2$ to $F' = 3$ transition. g_l depends on the dipole matrix element μ_a of the probed transition, which is different for the bright-MOT and dark-MOT cases [52]. The transition dipole moment with isotropic polarization for respective F and F' is the relevant μ_a, and the measured VRS is independent of the polarization of the probe beam [18]. The characterization of the bright MOT and the dark MOT was described in earlier work [43,45,47].
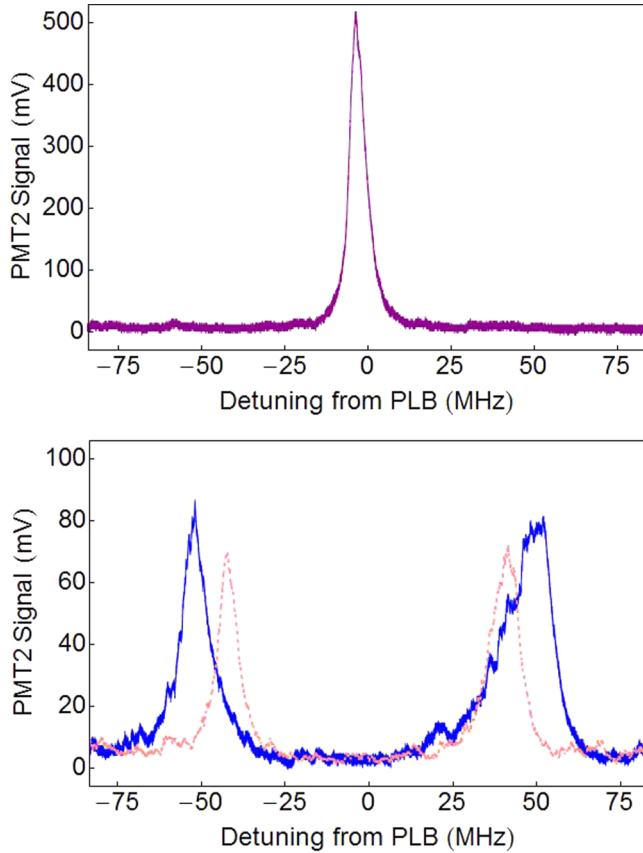
FIG. 3. Top: Empty cavity transmission for the LG_{00} cavity mode. Bottom: Transmission through the cavity with cocentered bright-MOT atoms. The solid blue curve shows VRS for the LG_{00} cavity mode, and the dashed pink curve shows VRS for the LG_{30} cavity mode. The VRS signal for the LG_{00} mode has a larger width and exhibits features of slight nonlinearity due to higher peak intensity as a result of a smaller mode cross section.

We have shown in earlier work that VRS measurements are independent of the polarization of the probe [18]. This is consistent with the present measurement. The *in situ* measurement of the VRS directly for the bright-MOT atoms is complicated by the coupling of MOT light into the near-resonant cavity mode [48]. Therefore, to measure the atom coupling variation with the probe light of specific spatial modes, we switch off the cooling lasers for 1 ms, keeping repumping lasers on, thereby optically pumping atoms into the $F = 3$ state, and within 0.5 ms scan the probe laser back and forth across the atom-cavity resonance, long before the atoms leave the trap region. The ballistic expansion of the atomic cloud during this time has been calculated [18] to be less than 1% of our MOT size. As the two VRS peaks occur at different times, the effect would be different on each. However, no corrections for this expansion have been made while presenting the results of this paper because this correction is substantially less than the statistical error of the measurements. For the dark MOT, since the atomic fluorescence is severely suppressed, *in situ* measurement of VRS can be done with the dark MOT [43,47].

The cavity probe light is taken from the output of a single-mode, polarization-maintaining fiber and has a Gaussian intensity profile. This TEM_{00} single-mode beam has good mode

matching with the LG_{00} cavity mode and has poor mode matching with higher-order LG_{l0} cavity modes. Therefore, higher input probe powers are required to obtain a measurable VRS signal with higher-order modes. This also limits the number of cavity modes up to which we can measure VRS. For the experiment the input light power is adjusted such that transmitted light output power through the empty cavity for different LG modes is constant and is sufficient to measure the VRS. This ensures that the conditions for measurement with different modes do not change significantly.

III. THEORETICAL ANALYSIS OF THE SYSTEM

For a beam propagating in the $\vec{z}$ direction the eigenmodes for transverse electric field functions in cylindrical coordinates (with radial index r, azimuthal index ϕ, and axial index z) can be expressed as $E(r, \phi, z) \propto \Psi_{lm}(r, \phi, z)\hat{\epsilon}$, where $\hat{\epsilon}$ is the unit vector in the polarization direction and $\Psi_{lm}(r, \phi, z)$ are Laguerre-Gauss functions [53] according to

$$\Psi_{lm}(r, \phi, z) = \frac{\omega(0)}{\omega(z)}\left(\frac{r\sqrt{2}}{\omega(z)}\right)^{|m|} e^{\left(\frac{-r^2}{\omega^2(z)}\right)} \mathbb{L}_l^{|m|}\left(\frac{2r^2}{\omega^2(z)}\right)$$
$$\times e^{i(kz-m\phi)} e^{i\left(\frac{kr^2}{2R(z)}\right)} e^{-i(2l+|m|+1)\tan^{-1}(z/z_R)}, \quad (1)$$

where k is the wave number, z_R is the Raleigh length, $\omega(z)$ is the waist of the LG_{00} mode, $R(z)$ is the radius of curvature of the cavity beam wavefront, $\mathbb{L}_l^m$ is the Laguerre polynomial with radial index l and azimuthal index m, and $\hat{z}$ is parallel to the optic axis of the cavity.

Within the cavity, the electric field in the transverse plane is given by $E_{cav}(r, \phi, z) = E^+(r, \phi, z) + E^-(r, \phi, z)$, which are the electric fields of forward- and reverse-propagating beams in the cavity, respectively. These cavity modes with $E_{cav} \propto [\Psi_{lm}(r, \phi, z) + \Psi_{l(-m)}(r, -\phi, -z)]$ are called Laguerre-Gauss modes. For the case of an aberration-free perfectly symmetric cavity, all LG_{lm} modes with equal value of $2l + |m|$ would be resonant for the same cavity length. The LG modes with $m \neq 0$ have an additional node at the center along with the l radial nodes at finite radii, and the size of this central node is larger for higher values of m. The VRS with the LG_{l0} mode is higher than the VRS due to the $LG_{(l-1)2}$ mode and so on for a Gaussian atomic density profile. In practical cavities, the phase of different modes with the same $2l + |m|$ would be slightly different due to aberrations, and hence, they would be resonant at slightly different cavity lengths [40], making it possible to stabilize any individual mode. In our experiment, we can adjust the mode-matching lens in Fig. 1 to stabilize only $m = 0$ modes by monitoring the CCD2 image and ensuring that there is no central dark spot. This ensures that the cavity modes in the present experiments have only the radial index l and the electric field inside the cavity is given by $E_{cav}(r, z) \propto \psi_l(r, z)\hat{\epsilon}$, where $\psi_l(r, z)$ is given by

$$\psi_l(r, z) = \frac{\omega(0)}{\omega(z)} e^{\left(\frac{-r^2}{\omega^2(z)}\right)} \mathbb{L}_l^0\left(\frac{2r^2}{\omega^2(z)}\right)$$
$$\times \cos\left[kz + \frac{kr^2}{2R(z)} - (2l+1)\tan^{-1}\left(\frac{z}{z_R}\right)\right]. \quad (2)$$
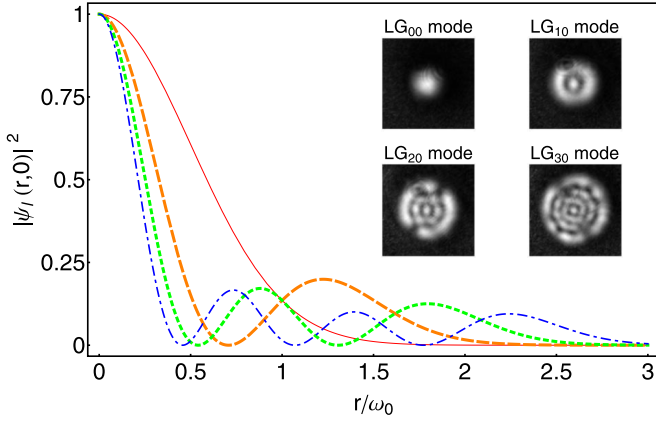
FIG. 4. Theoretical mode profile functions and images of transverse LG modes of the empty cavity, measured by imaging the probe light transmitted through the cavity. The solid red curve is for the LG_{00} mode, the dashed orange curve is for the LG_{10} mode, the dotted green curve is for the LG_{20} mode, and the dot-dashed blue curve is for LG_{30} mode.

The experimental images with the radial functional form of the intensity of the modes are illustrated in Fig. 4.

The number of atoms that couple with a particular cavity mode is determined by the overlap integral of the square of the mode function with the atomic density distribution. This is a fraction of the total atom number in the MOT N_{at}, and the fraction is dependent on the specific LG mode. The VRS due to collective strong coupling of atoms to the LG_{l0} mode of a cavity is given by [33,41]

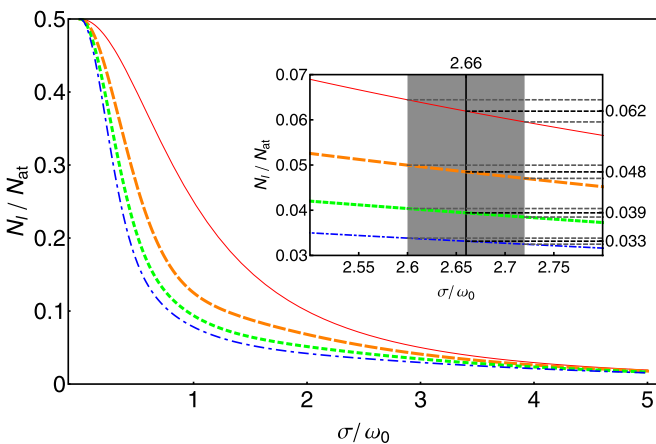$$2\hbar g_l = \mu_a \sqrt{\frac{2\hbar\omega_c N_l}{\epsilon_0 V_l}}, \tag{3}$$

FIG. 5. Ratio of atoms coupled to the LG_{l0} cavity mode N_l and the total number of atoms in the MOT N_{at} for different sizes of MOTs cocentered with the cavity. The solid red curve is for the LG_{00} mode, the dashed orange curve is for the LG_{10} mode, the dotted green curve is for the LG_{20} mode, and the dot-dashed blue curve is for the LG_{30} mode. The inset shows a zoomed-in version of the same curves around the value of σ/ω_0 measured from the CCD1 image of the bright MOT, 2.66 ± 0.06.

where V_l is the mode volume, N_l is the number of atoms coupled to the LG_{l0} mode, and they are given by

$$N_l = \int_{r=0}^{\infty} \int_{z=-L/2}^{L/2} \int_{\phi=0}^{2\pi} \rho(r, \phi, z)|\psi_l(r, z)|^2 d^3r, \tag{4}$$

$$V_l = \int_{r=0}^{\infty} \int_{z=-L/2}^{L/2} \int_{\phi=0}^{2\pi} |\psi_l(r, z)|^2 d^3r. \tag{5}$$

By solving Eq. (5), mode volumes V_l of all LG modes are obtained to be identically equal to $\pi\omega(0)^2 L/4$, where L is the cavity length. Single-atom-cavity coupling $\bar{g}$ is obtained by calculating g_l from Eq. (3) assuming $N_l = 1$. For our system, we calculate values of $\bar{g}$ to be ≈ 200.8 kHz for $F = 3$ to $F' = 4$ transition (PLB) and ≈ 96.6 kHz for $F = 2$ to $F' = 3$ transition (PLD) as the values of μ_a for these two cases are different.

In the case when the atomic density distribution ρ is a constant, the VRS $\Delta\nu = 2\hbar g_l$ becomes independent of l, which implies that the coupling to every LG mode is equal [26]. Alternatively, when ρ is not uniform, VRS for different LG modes will be different.

For a nonuniform, but regular, density profile of atoms, such as Gaussian distribution cocentered with the cavity, with peak density ρ_0 and $1/e^2$ radius $\sigma \ll L$, $\rho(r, \phi, z) = \rho_0 \exp[-2(z^2 + r^2)/\sigma^2]$, using Eqs. (2)–(5) and using $\omega(z) = \omega(0)$ and $\bar{r} = 2r^2/\omega(0)^2$, we get

$$\frac{g_{l+1}}{g_l} = \sqrt{\frac{\int_0^{\infty} e^{-(1+\alpha)\bar{r}} \left[\mathbb{L}_{l+1}^0(\bar{r})\right]^2 d\bar{r}}{\int_0^{\infty} e^{-(1+\alpha)\bar{r}} \left[\mathbb{L}_l^0(\bar{r})\right]^2 d\bar{r}}}. \tag{6}$$

Both the integrands in Eq. (6) are positive definite, the integral in the numerator is always smaller than that in the denominator, and for $\alpha = \frac{\omega_0^2}{4\sigma^2} \ll 1$, i.e., when $\omega_0 \ll 2\sigma$, $g_{(l+1)}/g_l \approx 1$, which is the uniform density of atoms case. A systematic decrease results in the VRS with higher-order modes (with an increase in the l index of the LG mode) for a Gaussian distribution when $\sigma \approx \omega_0$, see Fig. 5. So in this case of a Gaussian atomic distribution cocentered with the FP cavity, the change in the VRS with LG_{l0} can be used to measure the atom density distribution in the radial direction.

For a Gaussian density of atoms shifted radially from the axis of the cavity by a distance a, the number of atoms coupled to the LG_{l0} mode can be obtained by substituting $\rho'(r, \phi, z) = \rho_0 \exp\{-[(r-a)^2 + z^2]/\sigma^2\}$ in Eq. (3) and using $\bar{a} = 2(r - a)^2/\omega(0)^2$, which gives

$$N_l' \propto \int_0^{\infty} e^{-(\alpha\bar{a})} e^{-\bar{r}} \left[\mathbb{L}_l^0(\bar{r})\right]^2 d\bar{r}. \tag{7}$$

The integrand of Eq. (7) is positive definite and decreases as a increases. In this case the measured VRS due to the cavity-coupled atoms reduces very quickly as the cloud of atoms is displaced radially from the axis of the cavity. In the case of a single atom in the cavity, $N_l = |\Psi_{l0}(r_a, z_a)|^2$, where (r_a, ϕ_a, z_a) are the coordinates of the atom's position [1,5,6,9,37].

If the atomic ensemble is a uniform sphere of radius r_s and density ρ_s cocentered with the cavity,

$$\frac{N_l}{N_{at}} = \frac{2\pi\rho_s \int_0^{r_s} r\sqrt{(r_s^2 - r^2)} e^{-\bar{r}} \left[\mathbb{L}_l^0(\bar{r})\right]^2 dr}{(4\pi\rho_s r_s^3/3)}, \tag{8}$$
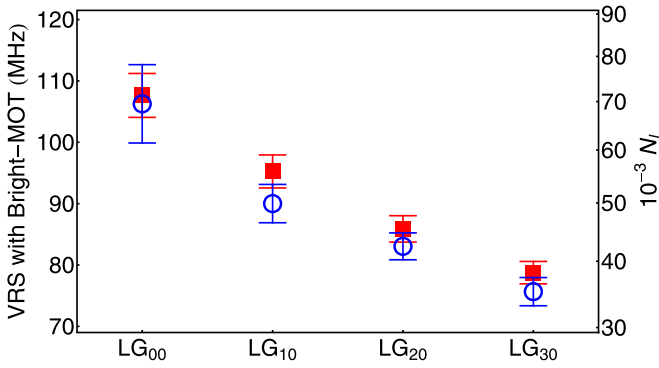
FIG. 6. VRS for different LG modes due to bright MOT measured on the $F = 3$ to $F' = 4$ transition. Blue circles are experimental values of measured VRS, and the blue error bars are one standard deviation. The red squares are calculated values of VRS, using N_{at} measured by the PMT1 signal and σ obtained from the Gaussian fit to the CCD1 image of the MOT, for different cavity modes. The red error bars include estimated errors in calculated VRS due to statistical and least-count errors in measured N_{at} and σ.

where N_{at} is the total number of atoms. However, when $L \gg r_s \gg \omega(0)$, for small values of l, we get $N_l = N_{at}$.

Thus, from the above analysis, we conclude that whether the density of atoms is uniform or a Gaussian distribution in an experiment which measures VRS can be determined. If the atomic ensemble is not radially symmetric, i.e., $\sigma_x \neq \sigma_y$, although the VRS with different LG modes can be numerically calculated, the ellipticity in the atomic density profile cannot be retrieved from the measured values of the VRS with different modes. Thus, we approximate the density of atoms to a spherical Gaussian distribution with $\sigma = (\sigma_x \sigma_y \sigma_z)^{1/3}$. For the bright-MOT case presented in this paper, we assume $\sigma_z = \sigma_y$ as the magnetic field gradient in the y and z directions is the same, as are the laser parameters, and we therefore use $\sigma = (\sigma_x \sigma_y^2)^{1/3}$.

IV. EXPERIMENTAL RESULTS AND DISCUSSION

The experimental results for the bright MOT are shown in Fig. 6. Here we see the VRS signal measured with a bright MOT and the effective number of atoms coupled to the cavity mode N_l as a function of changing LG modes. Care has been taken to ensure that the MOT is well centered by maximizing the VRS signal with the LG_{00} mode while ensuring the MOT is symmetric. It is observed that the measured VRS decreases as the l index increases for identical initial MOT atom number and MOT density profile. This matches the expected variation for a localized atomic ensemble with a three-dimensional Gaussian distribution of atoms, as expressed in Eq. (6). Calculated values of densities are expected to be higher than measured values for two reasons. First, we have neglected MOT expansion before measurement of VRS, and second, any finite amount of probe intensity leads to a reduced measure of VRS [47,49,54]. We have taken necessary measures to minimize these effects.

For the bright MOT, the best fits for parameter $\sigma = (\sigma_x \sigma_y^2)^{1/3}$ from the MOT image are found to be $209.3 \pm 3.9 \,\mu$m, while the least-count error due to the size of the
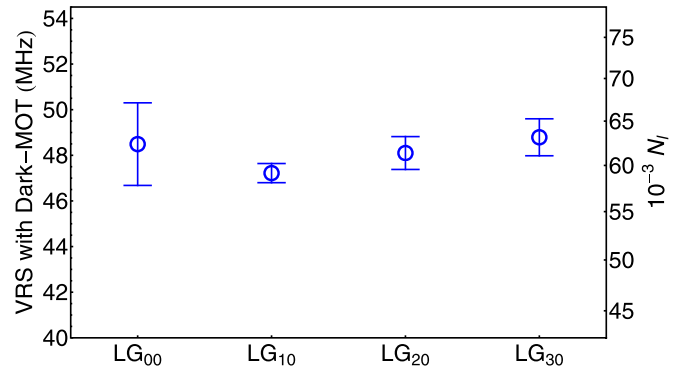

FIG. 7. VRS with a dark MOT for different LG modes measured on the $F = 2$ to $F' = 3$ transition. Blue circles are from experimental measurement of VRS, and the blue error bars are one standard deviation on either side of the mean value of corresponding measurements.

pixels in CCD1 is 4.6 μm. The total number of atoms in the MOT, $N_{at} = (1.16 \pm 0.03) \times 10^6$, is obtained from the PMT1 signal. This gives the peak atom density as $\rho_0 = (6.43 \pm 0.67) \times 10^{10}$ cm^{-3}. The VRS calculated for these values of N_{at} and σ using Eq. (3) are in good agreement, and this can be seen in Fig. 6. The possible source of systematic errors in the measurement of N_{at} due to cooling laser power fluctuations ($\pm 3\%$) is estimated to be less than 3%. However, accounting for a maximum possible error of ± 0.5 MHz in the measurement of the detuning of the cooling beams, we get a maximum potential systematic error of $\pm 8\%$ in the atom number measured through fluorescence. These errors are not shown in Fig. 6, where only the statistical errors and least-count errors are accounted for in the displayed error bars. In principle, measurements can be made with MOT atoms whose center is displaced from the cavity axis. However, shifting the MOT atoms spatially with respect to the cavity axis while maintaining the density profile is challenging. Such a measurement is much easier with dipole-trapped atoms within the cavity mode.

In the case of the dark MOT, atoms are optically pumped out of the cooling cycle, which allows for an *in situ* detection of atoms of a dark MOT using cavity coupling and VRS. For the dark MOT, the VRS for the different LG_{l0} modes used shows no statistically significant change, which is illustrated in Fig. 7. This is in stark contrast to the results for the bright MOT, where a monotonic decrease is seen in the VRS, with an increase in the l index. The constant VRS measured as a function of the different LG modes is consistent with the constant density of atoms in the central region of the dark MOT, within lengths of the order of ω_0, as discussed earlier.

Although the dark MOT cannot be imaged *in situ*, the two hollow repumping beams can be quickly changed to nonhollow beams, and the obtained PMT1 signal can be used to measure the total number of atoms in the dark MOT. Applying this method, we find the number of atoms in our dark MOT is $\approx 1.4 \times 10^6$. The measurement in Fig. 7 is a direct *in situ* measurement of dark-MOT atoms coupled to a cavity. The constant atom density is expected as the cooling in the central region of the dark MOT stops, and the energy of the atoms is sufficient to distribute them uniformly in the dark-spot region

of the MOT. Assuming uniform atomic density ρ_s, within a sphere of radius r_s and by numerically solving Eq. (8), we calculate the size of the dark MOT r_s to be 222 ± 7 μm and the density in the central region of the dark MOT ρ_s to be $3.1 \pm 0.3 \times 10^{10}$ cm^{-3}. The obtained value of r_s is ≈ 3 times $\omega(0)$, which is larger than the waist of the highest LG mode used.

V. CONCLUSIONS

In conclusion, we showed that the density distributions of atoms which are collectively strongly coupled to the cavity mode can be probed by varying the cavity spatial mode. The method works for trapped and free-flight atoms, as has been demonstrated. As different transverse modes have different spatial extents and spatial profiles, varying these directly samples the extended atomic distribution. Further, since the atoms are collectively strongly coupled to the cavity, the spatial measurement transforms into a frequency measurement, which is fast and robust in implementation. This is a robust method since sensitivity to the fluctuations in the atom number is suppressed due to the $\sqrt{N_c}$ dependence of the VRS. It should be kept in mind that if the density distribution is regular and cylindrically symmetric, then measurements with different transverse modes can measure the spatial density profile of the ensemble of atoms. In principle, when the entire distribution is shifted off axis, the density distribution can still be measured, although conducting such measurements with a MOT is very intricate as the atomic density profile changes as we shift the MOT. However, for dipole-trapped atoms, this method would be effective. In the case of ellipsoidal density distributions, the method does not apply. The method can be flexibly adapted to a wide variety of measurements in the future, expanding the toolbox of available techniques for the measurement of atoms coupled to a cavity.

In systems like a dark MOT, this method can be used to measure *in situ* density profiles, which are challenging to measure in other available methods like absorption imaging, where the resonant light used can alter the state preparation instantaneously and can perturb the atomic density profile. Since the cavity transmission is suppressed for resonant light due to VRS, the probe does not interfere with the state preparation of the atomic ensemble. A combination of spatial-mode-dependent measurement with a number-dependent frequency measurement can propel cavity-based measurements into new applications.

[1] C. J. Hood, M. S. Chapman, T. W. Lynn, and H. J. Kimble, Phys. Rev. Lett. **80**, 4157 (1998).

[2] A. D. Boozer, A. Boca, R. Miller, T. E. Northup, and H. J. Kimble, Phys. Rev. Lett. **97**, 083602 (2006).

[3] J. McKeever, A. Boca, A. D. Boozer, R. Miller, J. R. Buck, A. Kuzmich, and H. J. Kimble, Science **303**, 1992 (2004).

[4] P. Münstermann, T. Fischer, P. Pinkse, and G. Rempe, Opt. Commun. **159**, 63 (1999).

[5] P. Münstermann, T. Fischer, P. Maunz, P. W. H. Pinkse, and G. Rempe, Phys. Rev. Lett. **82**, 3791 (1999).

[6] H. Mabuchi, J. Ye, and H. J. Kimble, Appl. Phys. B **68**, 1095 (1999).

[7] J. M. Raimond, M. Brune, and S. Haroche, Rev. Mod. Phys. **73**, 565 (2001).

[8] T. Fischer, P. Maunz, P. W. H. Pinkse, T. Puppe, and G. Rempe, Phys. Rev. Lett. **88**, 163002 (2002).

[9] P. Horak, H. Ritsch, T. Fischer, P. Maunz, T. Puppe, P. W. H. Pinkse, and G. Rempe, Phys. Rev. Lett. **88**, 043601 (2002).

[10] H. W. Chan, A. T. Black, and V. Vuletić, Phys. Rev. Lett. **90**, 063003 (2003).

[11] V. Vuletić, J. K. Thompson, A. T. Black, and J. Simon, Phys. Rev. A **75**, 051405 (2007).

[12] I. B. Mekhov, C. Maschler, and H. Ritsch, Nat. Phys. **3**, 319 (2007).

[13] D. E. Chang, J. D. Thompson, H. Park, V. Vuletić, A. S. Zibrov, P. Zoller, and M. D. Lukin, Phys. Rev. Lett. **103**, 123004 (2009).

[14] D. R. Leibrandt, J. Labaziewicz, V. Vuletić, and I. L. Chuang, Phys. Rev. Lett. **103**, 103001 (2009).

[15] M. Koch, C. Sames, A. Kubanek, M. Apel, M. Balbach, A. Ourjoumtsev, P. W. H. Pinkse, and G. Rempe, Phys. Rev. Lett. **105**, 173003 (2010).

[16] M. H. Schleier-Smith, I. D. Leroux, H. Zhang, M. A. Van Camp, and V. Vuletić, Phys. Rev. Lett. **107**, 143005 (2011).

[17] K. W. Madison, Y. Wang, A. M. Rey, and K. Bongs, Annu. Rev. Cold At. Mol. **1**, 351 (2013).

[18] T. Ray, A. Sharma, S. Jyothi, and S. A. Rangwala, Phys. Rev. A **87**, 033832 (2013).

[19] R. Sawant, O. Dulieu, and S. A. Rangwala, Phys. Rev. A **97**, 063405 (2018).

[20] M. Keller, B. Lange, K. Hayasaka, W. Lange, and H. Walther, Nature (London) **431**, 1075 (2004).

[21] R. Miller, T. E. Northup, K. M. Birnbaum, A. Boca, A. D. Boozer, and H. J. Kimble, J. Phys. B **38**, S551 (2005).

[22] A. K. Tuchman, R. Long, G. Vrijsen, J. Boudet, J. Lee, and M. A. Kasevich, Phys. Rev. A **74**, 053821 (2006).

[23] G. Hernandez, J. Zhang, and Y. Zhu, Phys. Rev. A **76**, 053814 (2007).

[24] P. F. Herskind, A. Dantan, J. P. Marler, M. Albert, and M. Drewsen, Nat. Phys. **5**, 494 (2009).

[25] C. Guerlin, E. Brion, T. Esslinger, and K. Mølmer, Phys. Rev. A **82**, 053832 (2010).

[26] M. Albert, J. P. Marler, P. F. Herskind, A. Dantan, and M. Drewsen, Phys. Rev. A **85**, 023818 (2012).

[27] H. Ritsch, P. Domokos, F. Brennecke, and T. Esslinger, Rev. Mod. Phys. **85**, 553 (2013).

[28] L. Karpa, A. Bylinskii, D. Gangloff, M. Cetina, and V. Vuletić, Phys. Rev. Lett. **111**, 163002 (2013).

[29] A. Wickenbrock, M. Hemmerling, G. R. M. Robb, C. Emary, and F. Renzoni, Phys. Rev. A **87**, 043817 (2013).

[30] S. Begley, M. Vogt, G. K. Gulati, H. Takahashi, and M. Keller, Phys. Rev. Lett. **116**, 223001 (2016).

[31] E. T. Jaynes and F. W. Cummings, Proc. IEEE **51**, 89 (1963).

[32] M. Tavis and F. W. Cummings, Phys. Rev. **170**, 379 (1968).

[33] *Cavity Quantum Electrodynamics*, edited by P. R. Berman, Advances in Atomic, Molecular and Optical Physics (Academic, San-Diego, 1994).

[34] E. A. Hinds, Adv. At., Mol., Opt. Phys. **28**, 237 (1990).

[35] D. Meschede, H. Walther, and G. Müller, Phys. Rev. Lett. **54**, 551 (1985).

[36] G. Rempe, H. Walther, and N. Klein, Phys. Rev. Lett. **58**, 353 (1987).

[37] R. J. Thompson, G. Rempe, and H. J. Kimble, Phys. Rev. Lett. **68**, 1132 (1992).

[38] K. M. Birnbaum, A. Boca, R. Miller, A. D. Boozer, T. E. Northup, and H. J. Kimble, Nature (London) **436**, 87 (2005).

[39] J. D. Sterk, L. Luo, T. A. Manning, P. Maunz, and C. Monroe, Phys. Rev. A **85**, 062308 (2012).

[40] J. Du, W. Li, R. Wen, G. Li, P. Zhang, and T. Zhang, Appl. Phys. Lett. **103**, 083117 (2013).

[41] M. Albert, Ph.D. thesis, University of Aarhus, Denmark, 2011.

[42] M. Cetina, A. Bylinskii, L. Karpa, D. Gangloff, K. M. Beck, Y. Ge, M. Scholz, A. T. Grier, I. Chuang, and V. Vuletić, New J. Phys. **15**, 053001 (2013).

[43] S. Dutta and S. A. Rangwala, Phys. Rev. A **94**, 053841 (2016).

[44] M. Albert, A. Dantan, and M. Drewsen, Nat. Photonics **5**, 633 (2011).

[45] T. Ray, S. Jyothi, N. B. Ram, and S. A. Rangwala, Appl. Phys. B **114**, 267 (2014).

[46] S. Jyothi, T. Ray, B. Ram, and S. Rangwala, Hybrid ion atom and light trap, in *Ion Traps for Tomorrow's Applications* (IOS Press, 2015), Vol. 189, pp. 269–287.

[47] S. Dutta and S. A. Rangwala, Appl. Phys. Lett. **110**, 121107 (2017).

[48] R. Sawant and S. A. Rangwala, Sci. Rep. **7**, 11432 (2017).

[49] J. Gripp, S. L. Mielke, and L. A. Orozco, Phys. Rev. A **56**, 3262 (1997).

[50] S. Haroche and J.-M. Raimond, in *Exploring the Quantum* (Oxford University Press, Oxford, 2006), Chap. 5, p. 243.

[51] A. Dantan, M. Albert, J. P. Marler, P. F. Herskind, and M. Drewsen, Phys. Rev. A **80**, 041802 (2009).

[52] D. A. Steck, "Rubidium 85 D Line Data," available online at http://steck.us/alkalidata (revision 2.1.6, 20 September 2013).

[53] G. Goubau and F. Schwering, IRE Trans. Antennas Propag. **9**, 248 (1961).

[54] J. Gripp, S. L. Mielke, L. A. Orozco, and H. J. Carmichael, Phys. Rev. A **54**, R3746 (1996).